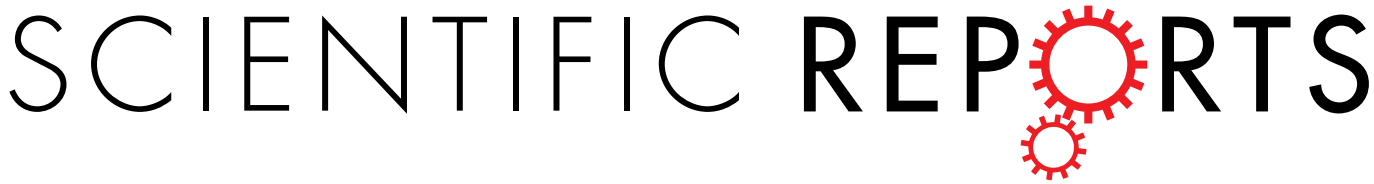

OPEN

Bio-Derived, Binderless, Hierarchically Porous Carbon Anodes for Li-ion Batteries

Received: 08 May 2015
Accepted: 03 September 2015
Published: 29 September 2015

Brennan Campbell[1], Robert Ionescu[1], Zachary Favors[1], Cengiz S. Ozkan[1] & Mihrimah Ozkan[2]

Here we explore the electrochemical performance of pyrolyzed skins from the species *A. bisporus*, also known as the Portobello mushroom, as free-standing, binder-free, and current collector-free Li-ion battery anodes. At temperatures above 900 °C, the biomass-derived carbon nanoribbon-like architectures undergo unique processes to become hierarchically porous. During heat-treatment, the oxygen and heteroatom-rich organics and potassium compounds naturally present in the mushroom skins play a mutual role in creating inner void spaces throughout the resulting carbon nanoribbons, which is a process analogous to KOH-activation of carbon materials seen in literature. The pores formed in the pyrolytic carbon nanoribbons range in size from sub-nanometer to tens of nanometers, making the nanoribbons micro, meso, and macroporous. Detailed studies were conducted on the carbon nanoribbons using SEM and TEM to study morphology, as well as XRD and EDS to study composition. The self-supporting nanoribbon anodes demonstrate significant capacity increase as they undergo additional charge/discharge cycles. After a pyrolysis temperature of 1100 °C, the pristine anodes achieve over 260 mAh/g after 700 cycles and a Coulombic efficiency of 101.1%, without the use of harmful solvents or chemical activation agents.

Carbon materials are of great importance to a range of battery chemistries. Carbon is the most versatile element on the periodic table, and its various allotropes make for highly diverse properties and applications. In Li-ion batteries, carbon has been studied for decades. The current industry standard for rechargeable Li-ion battery anodes is synthetic graphite. While graphite has commercially desirable attributes, such as a high cycling stability and low hysteresis, it comes with its own trade-offs. The disadvantages of graphite are that it is relatively expensive to make and has a relatively low lithium storage capacity per carbon weight (LiC_6)[1]. Alternatives to graphitic carbons for Li-ion anodes are hard carbons and soft carbons, which can be synthesized in a number of ways. A traditional form of hard carbon synthesis involves the pyrolysis of sucrose, a natural organic sugar. Studies conducted by Buiel and Dahn show that hard carbon anodes yield higher specific capacities than graphitic structures (over 500 mAh/g). However, they tend to have significant irreversible capacity, owing to lithium's reactivity with both the electrolyte and the surface functional groups of the carbon structure which form after pyrolysis[2]. In terms of commercializing new forms of carbon for Li-ion batteries, naturally-derived carbon precursors must be explored. Activated carbons are also showing incredible promise for implementation as scalable, commercially-viable Li-ion anodes. Activated carbons are most commonly produced from exposure to a concentrated KOH solution, or other chemical activating agents. KOH treatment generates additional mesopores and/or micropores after thermal activation; the resulting defects encourage higher capacities by allowing additional lithium insertion into the carbon[3]. A traditional method for activating carbon involves submersion in a KOH bath, followed by a high-temperature heat-treatment. For KOH activation, two modes of action are thought to be at play for pore generation, such as reaction of carbon with

[1]Materials Science and Engineering Program, Department of Mechanical Engineering, University of California, Riverside, Riverside, CA 92521, USA. [2]Department of Chemistry, Department of Electrical Engineering, University of California, Riverside, Riverside, CA 92521, USA. Correspondence and requests for materials should be addressed to C.S.O. (email: cozkan@engr.ucr.edu) or M.O. (email: mihri@ece.ucr.edu)

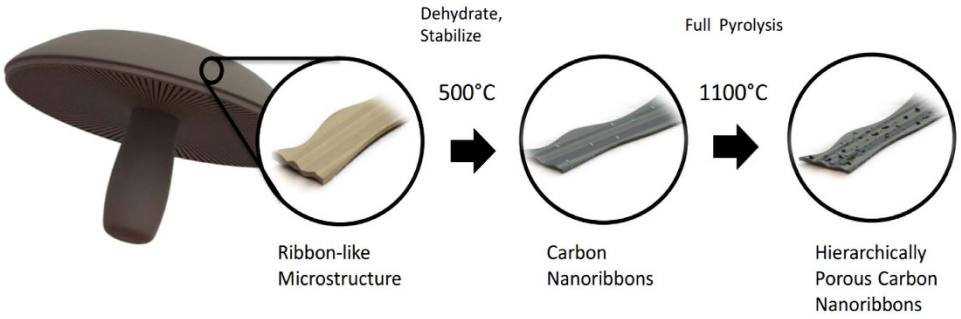

Figure 1. Schematic illustration of the process of obtaining Portobello mushroom skin-derived, hierarchically porous carbon nanoribbons used as free-standing, binder-free, current collector-free carbon anodes. Lauro Zavala is credited for the contribution of this artwork.

metallic K, as well as CO and CO_2 formation[3,4]. Hwang, *et al.* explored the efficacy of coffee shell-derived activated carbon as a Li-ion anode, which they activated using KOH and an array of other activating agents. This process produced an anode with a nearly 300 mAh/g reversible capacity over 15 cycles, with an impressive initial capacity of over 1100 mAh/g[5]. There are several nuances to characterizing high-performance biomass-derived carbon anodes for Li-ion batteries, due to their complex organic compositions. Biomass-derived electrode materials are of great interest because of their high carbon content, low cost, and environmental benignity[6].

In this work, we study the electrochemical performance of pyrolytic carbons derived from the cap skin tissue (CST) of the mature fruiting body of the fungus, *A. bisporus*, otherwise known as the Portobello mushroom (PM). Our studies of the PM CSTs have revealed compelling microstructural features after anoxic carbonization. Specifically, we discovered that the pyrolyzed PM CST formed high aspect-ratio carbon nanoribbons. Additionally, we confirmed remarkably high concentrations of salts after carbonization, primarily KCl. Further, PM CSTs were examined after various pyrolysis temperatures (PTs) to compare microstructural and compositional changes with corresponding electrochemical behaviour. The purpose of this method is to observe the true performance of bio-derived structures as battery electrodes (i.e., without binder, conductive additive, etc.), and to examine the characteristics of the resulting pristine carbon. To this end, the PM CST anodes were placed in a Li-ion battery half-cell configuration, completely as-synthesized. In further SEM studies, the PM CSTs manifested hierarchical porosity after PT above 900 °C, showing macro, meso, and micropores, as illustrated in the schematic in Fig. 1. This raised an interesting possibility with this unique material; PM CSTs may, due to their unusually high K concentration, be self-activating. However, synthetic processes need to be optimized to expose the microchannels or worm-like micropores formed during pyrolysis, and thereby increase the measurable surface area. These novel PM CST anodes are binder-free, requiring zero polymers or conductive additives, to attain capacities that are comparable to practical graphite-based electrodes. Binder-free Li-ion electrodes are far superior to graphite-based electrodes, due to their higher utilization of total electrode weight as active material, and minimal processing. In turn, this translates to batteries with higher energy density, lower cost, and lower environmental impact.

Results

Structural characterization was conducted on the PM CSTs using SEM, observing pyrolysis-induced morphological transformations at the micro- and nanoscale. From the micrographs in Fig. 2, it can be seen that the common microstructural feature is nanoribbons, with a sometimes wrinkled appearance. They make up an extremely thin, secondary electron-transparent array of interconnected, branching ribbons with widths of about 10 μm, lengths of several tens of microns or longer, and a thickness of about 20–100 nm. A key structural difference making 700CSTs (Fig. 2a,b) distinct from 900CSTs (Fig. 2c,d) and 1100CSTs (Fig. 2e,f) is the presence of round salt pockets. These salt pockets are thought to form during heating, as water escapes and naturally-present biological salts aggregate, both within the chitin-based organics, and on the surface. At temperatures above 900 °C, these salt pockets disappear, having exceeded the melting points of most salts present. It should also be noted that, especially in Fig. 2a,e, the nanoribbons form a network. There is also layering and/or pseudo-layering, as evidenced in Fig. 2c, which shows a lateral view of the layered ribbon networks.

Observations were also made on higher-magnification SEM micrographs of the various PM CSTs. As mentioned, biological salts (primarily KCl) organize in pockets of varying sizes, and begin to create additional void space at 700 °C. However, the melting point of KCl is 770 °C, and above this temperature the salts escape the carbon structure more completely. As captured in Fig. 3a,b, salt deposits are still present at the surface of the nanoribbons, having a wide diameter distribution (although some pores are still formed). Beginning in Fig. 3c,d, no surface salts or salt pockets are present, and instead there is a hierarchically porous texture. Pores observable from SEM have diameters between 26 nm or higher, down to

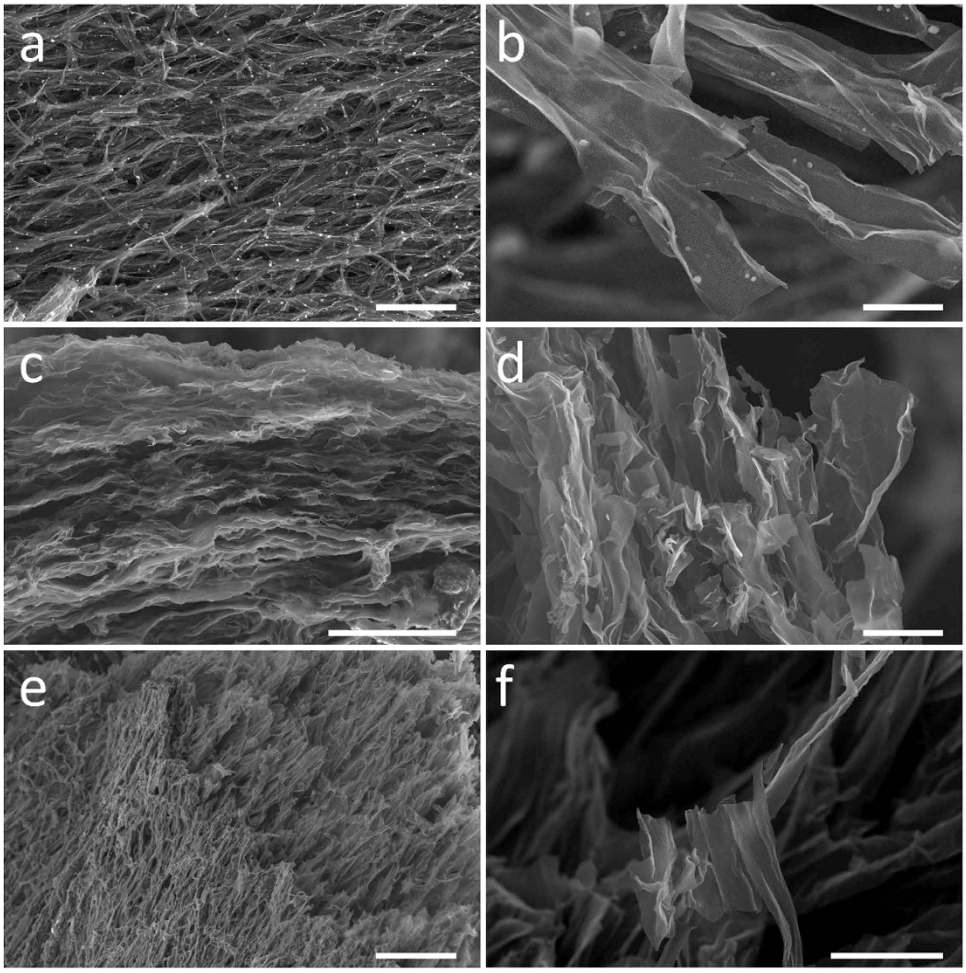

Figure 2. Low to high magnification SEM of PM CST anodes heat-treated at 700 °C **(a,b)**, 900 °C **(c,d)**, and 1100 °C **(e,f)** (scale bars for **(a–f)**, respectively: 100 μm, 10 μm, 50 μm, 10 μm, 100 μm, and 10 μm).

an observable 6 nm, which is the lowest feature size observable from the SEM images. From this data, it is confirmed that this material becomes mesoporous upon pyrolysis, with pore sizes of 6–26 nm observable by SEM. Images in Fig. 3e,f, representing the 1100CSTs, display an even wider range of porosity than the 900CSTs, with macropores of up to 100 nm in diameter. To confirm that porosity exists throughout the bulk of the nanoribbons, rather than solely on the surface, cross-sections of the nanoribbons were captured under SEM, shown in Fig. 3d,f. In these images, the presence of pores is evident throughout the entire thickness of the nanoribbons.

Detailed transmission electron microscopy (TEM) analysis was also conducted on the 1100CSTs, since they were both the highest performing anode material, and displayed the highest apparent porosity from SEM. The microstructure seen in the lower-magnification images (Fig. 4a,b) is consistent with what is seen in SEM, which is a thin, highly mesoporous nanoribbon architecture. The range of pore size is confirmed from Fig. 4b,d,f, identifying macropores and mesopores. Remarkably, TEM analysis also confirms the presence of worm or channel-shaped micropores, as observed in Fig. 4f. The low thickness of the ribbon is observed from the transparency of the structure in Fig. 4a, wherein the lacey carbon from the TEM grid is visible from beneath the sample. The general shape of the meso- and macropores of the nanoribbons is circular, information which supports the idea that salt pocket formation, and subsequent melting induces this type of void space generation. On the other hand, it is hypothesized that the worm-like micropores captured in Fig. 4f are generated through an activation-like process. N_2 adsorption/desorption isotherms show a long, flat plateau for adsorption and desorption, and a significant hysteresis (a characteristic of mesoporous and/or microporous carbons). The BET surface area was measured at 19.6 m^2/g, which is a discrepancy in relation to the isotherm and TEM data; this points the prevalence of "blind," or inaccessible pores formed in the 1100CSTs, which then become accessed after deep cycling. Moreover, our leading hypothesis is that oxygenated organics (polysaccharides, oligosaccharides, amino acids, DNA), combined with the unusually high K concentration, may lead to carbonate formation, and subsequent CO_2 generation; this is that basis of chemical activation, or a similar mechanism.

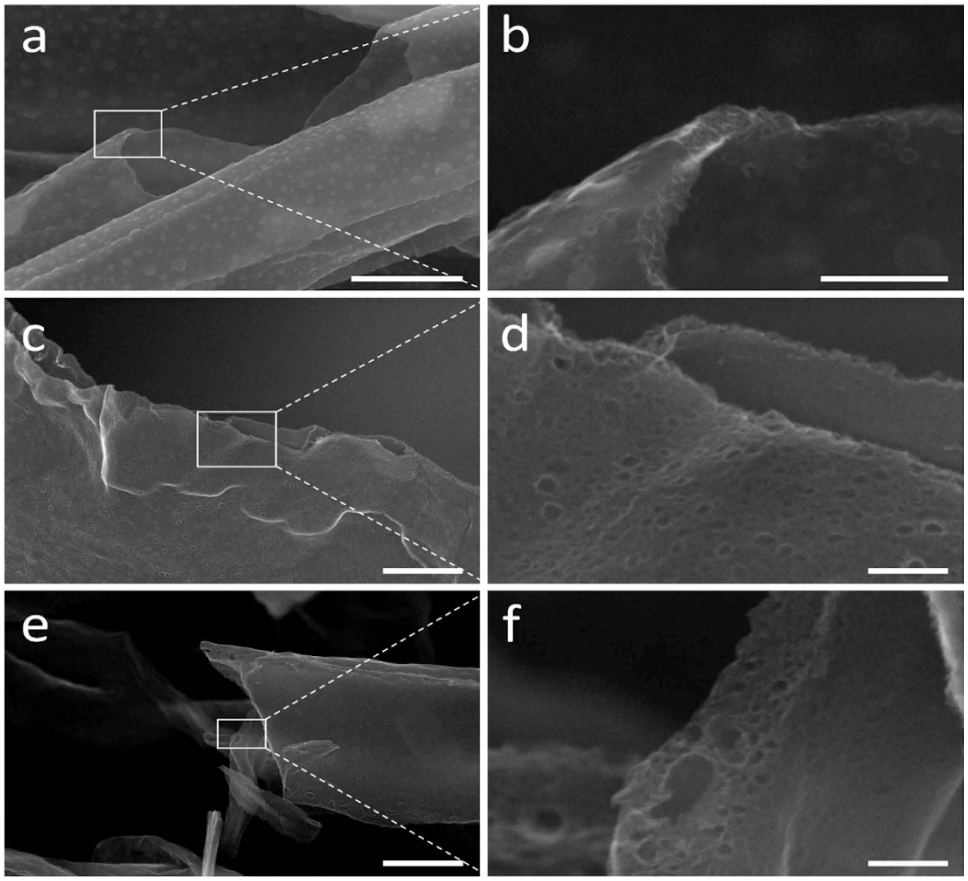

Figure 3. Low to high magnification SEM showing the increasing degree of porosity of PM CST nanoribbons as temperature increases, including sample heat-treated at 700 °C **(a,b)**, 900 °C **(c,d)**, and 1100 °C **(e,f)** (Scale bars for **(a–f)**, respectively: 1 μm, 200 nm, 500 nm, 100 nm, 1 μm, and 100 nm).

The phenomenon of small, biological salt pockets causing void spaces of various sizes, from the macroporous to microporous domains, leads us to propose that high PT-pyrolyzed PM CSTs are inherently a self-activating material, by a complex set of mechanisms. It is highly advantageous to have a material that can be naturally primed for optimal performance by simply applying heat-treatment. At PT of 1100 °C, macropores form, facilitating electrolyte infiltration and hence electrolyte interaction with high surface-area hard carbon (shown to be higher capacity than graphite, gravimetrically)[7]. Mesoporous carbons have been shown to perform with excellent stability over long-cycling in literature[8], however, harsh chemical methods are required to achieve such performance. Hierarchically porous carbons, also achieved by many activation methods, tend to improve ion diffusion rates, and expose additional active material for reversible capacity enhancement[9–10].

Spectral data was obtained from the PM CSTs after PTs of 700–1100 °C to analyze elemental composition by point-ID energy dispersive x-ray spectroscopy (EDS), and phase information using x-ray diffractometry (XRD) of the free-standing anodes. From Fig. 5a, XRD patterns show the transition from large KCl peaks for the 700CSTs (blue), to the 1100CSTs (black) with no visible peaks of crystalline inorganics. The prevailing model for KOH-activation is shown in Eqn. (1) and (2). At temperatures above 400 °C Eqn. (1) occurs, and above 700 °C Eqn. (2) occurs (gasification of CO_2 occurs throughout this process)[10]. Further, K_2O from Eqn. (2) continues to be reduced by carbon to metallic K at above 700 °C. A physical means of activation then occurs, when metallic K diffuses into carbon, expanding the lattice[10]. Considering the classical chemical and physical models for KOH-activation, it is likely that the biological salts present in the PM provide suitable precursors for similar activation mechanisms. With salt deposits of various sizes composed of KCl, and likely a host of carbonates and phosphates, the PM is an ideal self-activating carbon precursor for PTs above 900 °C.

$$6KOH + 2C \rightarrow 2K + 3H_2 + 2K_2CO_3 \quad (1)$$

$$K_2CO_3 \rightarrow K_2O + CO_2 \quad (2)$$

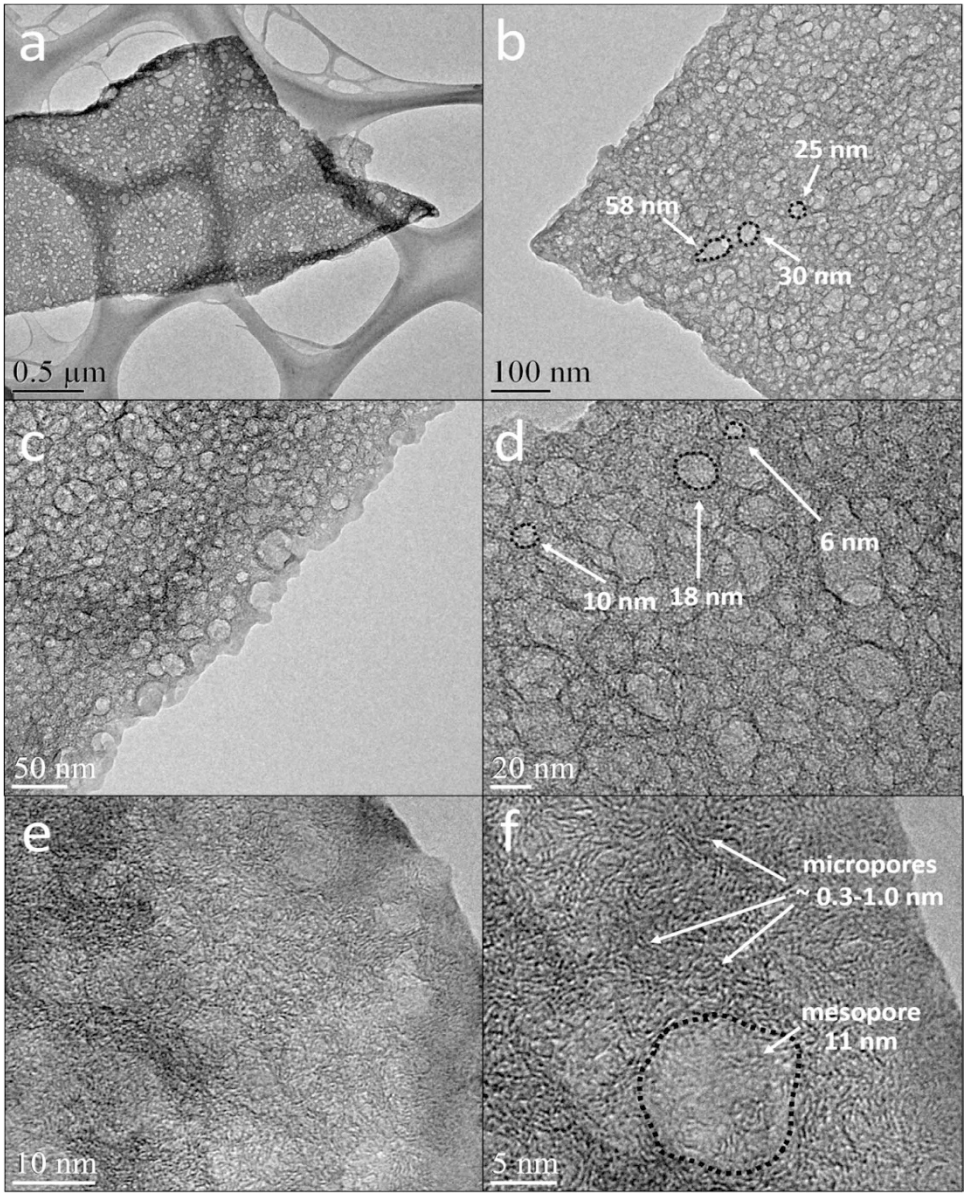

Figure 4. TEM of pristine PM 1100CST hierarchically porous nanoribbons, showing macroporosity **(a,b)**, mesoporosity **(c,d)** and worm-like microporosity **(e,f)**.

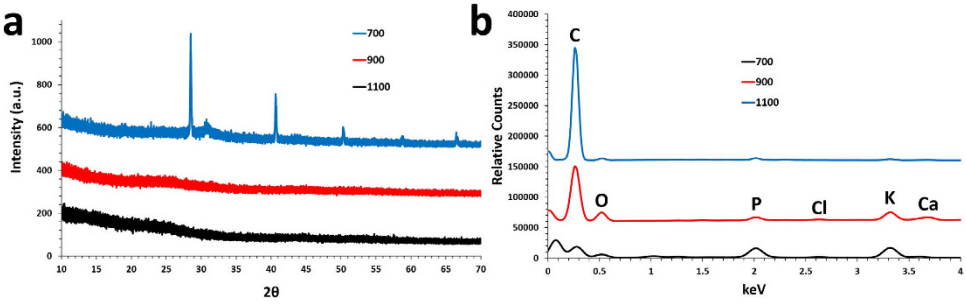

Figure 5. Spectral data of the pristine, free-standing PM CSTs at various PTs, including XRD **(a)** and point-ID EDS **(b)**.

The EDS spectrum is included in Fig. 5b, which clearly shows the diminishing metal salts as the PT increases from 700–1100 °C. The free-standing electrodes which result from pyrolysis are used as-synthesized for electrochemical characterization. Naturally, as the wt.% of heteroatoms and inorganic material is reduced in the electrodes, the specific cycling capacity increases. Although EDS results vary slightly from sample to sample (since no two biological specimens are compositionally precisely the same), an average of ~50 wt.% carbon was found in 700CSTs, ~70 wt.% carbon in 900CSTs, and ~90 wt.% carbon in 1100CSTs. While a main mode of oxygen reduction is through gasification and formation of CO_2, an additional mode is thought to be the melting of inorganics and salts. To observe any differences in battery performance on the carbon anodes due to surface functionalization, some 1100CSTs were submerged in a KOH bath for several hours at 80 °C before electrochemical characterization, and denoted as "KOH1100CST."

Discussion

The specific capacity increase from 700CSTs to 1100CSTs is both due to carbon purification from high PT, and from the proposed natural self-activation, allowing for increased electrolyte infiltration and utilization of active mass. The specific capacities of each sample increases over time, suggesting that the initially unexposed meso- and micropores become more accessible after repeated cycling. It should be specifically noted that the capacity of the 1100CSTs and KOH1100CSTs begin to converge near the 270th cycle. The large difference in discharge capacity between 1100CSTs and KOH1100CSTs from cycle number 1 and 60 may be attributed to initial improved wetting from surface functionalization with hydroxyl and/or carboxyl functional groups. In the long-term, the full capacity may not be significantly affected by these surface groups; in fact, after 500 cycles the non-KOH-wetted 1100CSTs achieve significantly higher capacity at a higher rate. While all four PM CSTs exhibit a very gradual increase in capacity over time, the 1100CSTs maintain the steepest incline.

As previously explained, there are likely[11] multiple modes of action by which this hard carbon-like material becomes activated. A complex mixture of salts, including KCl, NaCl, and likely phosphates[12], coupled with organics their respective heteroatoms, is undergoing reactions above 700 °C that induce CO_2 gasification, as well as metallic K diffusion and carbon lattice expansion. Most interestingly, the more pronounced capacity incline of the 1100CSTs and KOH1100CSTs strongly indicates that the micropores are becoming more accessible to the electrolyte with each subsequent oxidation/reduction reaction of the anode (reactions which initially are taking place at the electrode surface). As the micropores become more accessible to the electrolyte, the effective specific active mass increases, therefore increasing the specific capacity over time. Figure 6a shows that by the 700th cycle, 700CSTs, 900CSTs, 1100CSTs, and KOH1100CSTs exhibit 121.6 mAh/g, 157.5 mAh/g, 233.8 mAh/g, and 260.1 mAh/g, respectively. Therefore, a capacity increase of over 138 mAh/g from PT 700–1100 °C is achieved for the free-standing carbon anodes, with the 1100CSTs outperforming the KOH1100CSTs for more than half the current life of the battery. If calculated based on the approximate wt.% of carbon in the 1100CST cathode, the specific discharge capacity is 289 mAh/g, which is expected to increase to beyond 300 mAh/g at its current rate of capacity increase. The first discharge/charge cycle for this experiment was run at a rate of C/10, while all subsequent cycles were run at C/5, based on a theoretical limit of 500 mAh/g. The initial discharge capacity (out of range for Fig. 6a,g) for 700CSTs, 900CSTs, 1100CSTs, and KOH1100CSTs are 429.6 mAh/g, 617.8 mAh/g, 771.3 mAh/g, and 630.9 mAh/g, respectively. A relatively large irreversible initial capacity loss is exhibited for each of the PM CSTs, which is highly characteristic of hard carbon structures.

The Coulombic efficiency (CE) plots of all PM CSTs are shown in Fig. 6b, including the KOH1100CSTs (linear trend lines shown in their respective colors for distinction). Contrary to what was expected, the 700CSTs actually demonstrated the 2nd highest overall CE, achieving higher than both the 1100CSTs and 900CSTs. The higher CE in 700CSTs may explained in two parts: a) the samples, with the exception of the KOH1100CSTs, were unwashed before placing in coin cells, and b) the electrolyte has relatively low access to the carbon-protected salts that are, below 900 °C, still trapped in pockets. Since the 900CSTs and 1100CSTs have exposed the majority of the salts, and were also unwashed, the CE may be adversely affected by the electrolyte interaction with any residual salts. Overall, the average CE between cycles 30 and 700 for 700CSTs, 900CSTs, 1100CSTs, and KOH1100CSTs are 99.79, 99.51, 99.75 and 100.37%, respectively.

Cyclic voltammetry (CV) was performed on the PM CSTs at PTs from 700–1100 °C, including the KOH1100CSTs, for 11 cycles. The scanning rate used for all CV measurements was 0.1 mV/s. For each of the curves in Fig. 6c–f, the peak in the initial cycle at ~0.5 V is indicative of the solid-electrolyte interphase (SEI) layer formation. This reaction stabilizes relatively quickly with the 2nd cycle and subsequent cycles at around 0.2 V. The 700CST shows a less pronounced SEI formation peak compared to the higher PT samples, which corresponds well with the smaller irreversible capacity loss from the 1st cycle. During charging, each PM CST exhibits a delithiation peak for cycles 2–11 at about 0.3 V. This peak is much more pronounced after PTs above 900 °C; the current increases with each subsequent cycle.

Voltage profiles were obtained from charge/discharge cycling data for cycles 1, 10 and 50, for all PM CST anodes. Voltage profiles are shown for 700CST, 900CST, 1100CST, and KOH1100CST in Fig. 7a–d, respectively. As the PT of the PM CSTs increases, the voltage plateau extends upon each step, as in

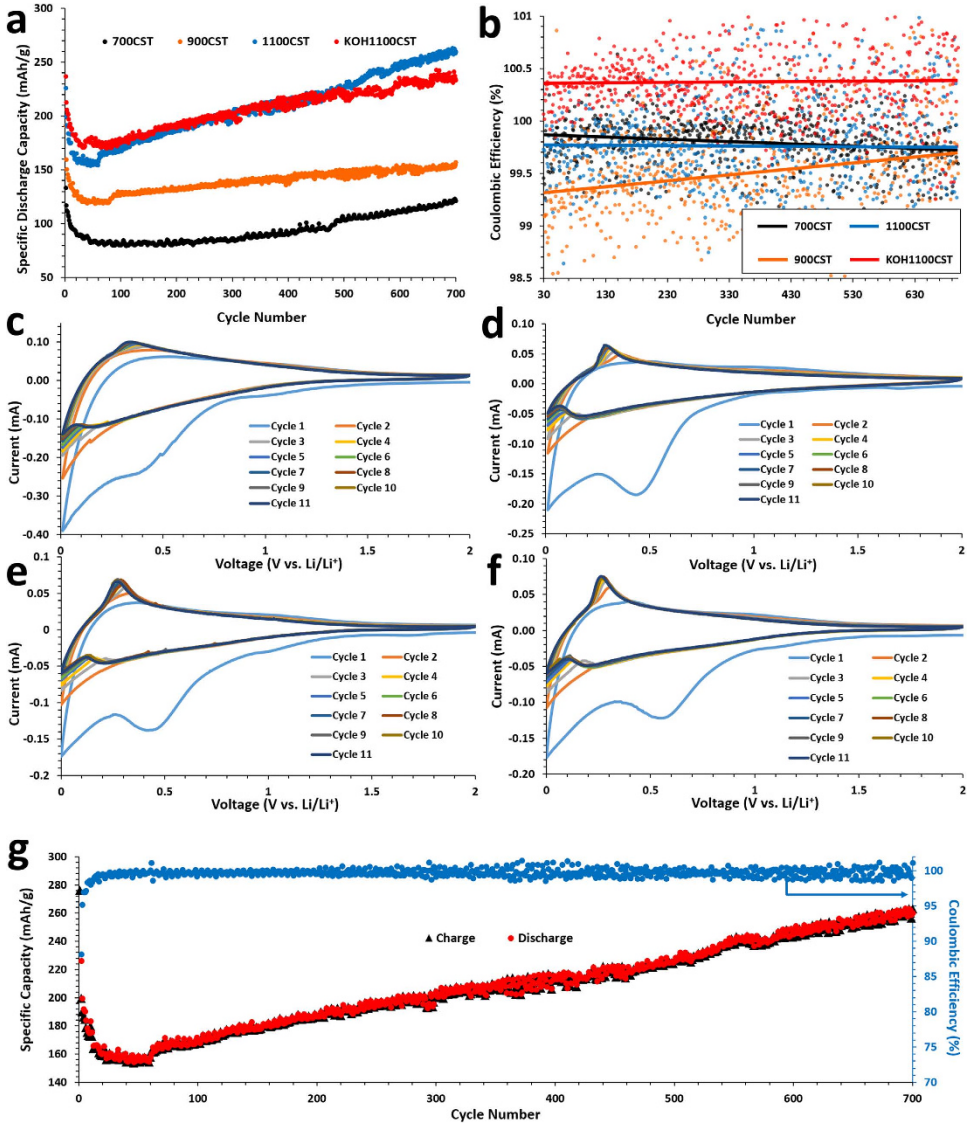

Figure 6. Electrochemical performance data of PM CSTs, including discharge plots **(a)**, Coulombic efficiency plots **(b)**, CV curves from cycles 1–11 for 700CST **(c)**, 900CST (d), 1100CST **(e)**, and KOH1100CST **(f)**, and finally the charge/discharge plot with corresponding Coulombic efficiency for 1100CST **(g)**.

between 700–900 °C and 900–1100 °C. The exception is the initial cycle, shown to actually decrease after KOH-wetting (Fig. 7c,d). The voltage plateaus of PM CSTs agree well with their respective CV measurements, with the operating voltage up to about 1.5 V.

In conclusion, a novel free-standing, binder-free, additive-free carbon anode was synthesized via pyrolysis at various temperatures, with cap skin tissue (CST) from mature *A. bisporus* (Portobello mushroom (PM)) as the precursor. The resulting morphology of the PM CST anodes, above PT of 900 °C, is an interconnected network of hierarchically porous carbon nanoribbons. The electrochemical behaviour of PM CSTs vs. lithium was studied, exhibiting advanced performance as a free-standing anode for 700 cycles. Structural characterization by SEM indicates the PM CSTs treated at or above 900 °C become hierarchically porous, with a continuous increase in specific capacity, thus leading to the proposal that the material is self-activating due to its unusually high concentration of natural K. The performance of the PM CSTs heated to 1100 °C was also analyzed after wetting with a high-concentration KOH bath. While wetting improved the capacity for the first 50 or so cycles, it became fairly negligible in later cycles compared to the non-wetted 1100CSTs. This work will lead to new explorations into free-standing biomass-derived hierarchically porous materials for energy storage that are high-performance, extremely cheap, and environmentally benign.

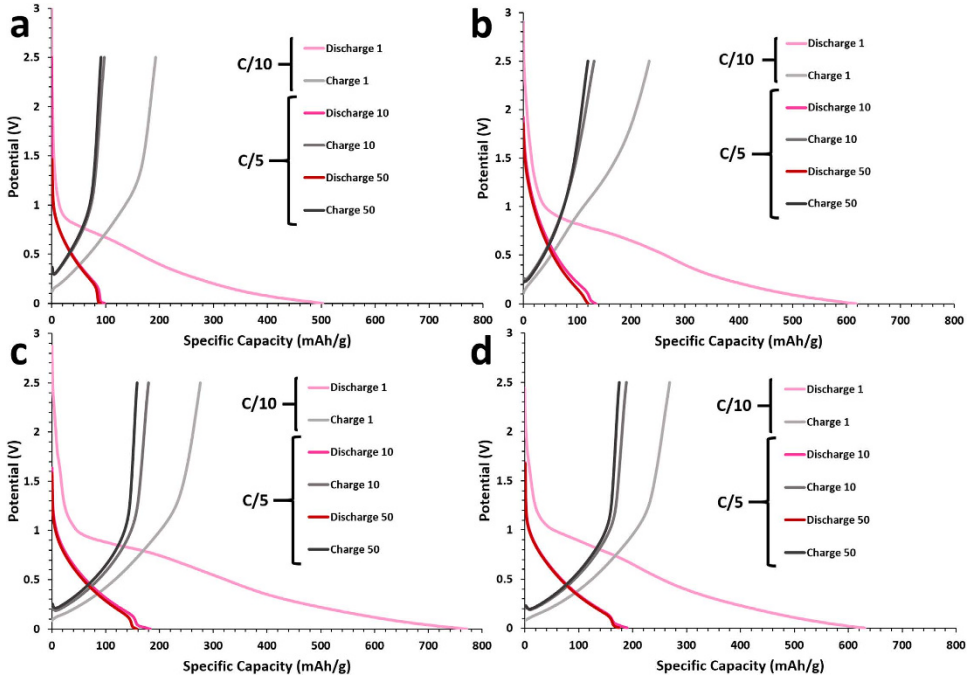

Figure 7. Voltage profiles of cycles 1, 10 and 50, for PM CSTs, including 700CST **(a)**, 900CST **(b)**, 1100CST **(c)**, and KOH1100CST **(d)**.

Methods section

Typical experiments entailed the following: organic PMs were purchased from local markets and cleaned with DI H_2O. The CSTs were peeled from the caps of the PMs and set aside. Razor blades were then used to slice the CSTs into quartered sections. Using a 15 mm hole punch, disk-shaped samples were obtained from CSTs. All samples were placed on silicon wafer substrates, and dried overnight at 80 °C in a vacuum oven. Before transferring the dried samples to a high-temperature tube furnace, an additional silicon wafer was placed on top of the samples to keep them relatively flat during heat-treatment. At 700 Torr, Ar gas was flowed at 300 sccm while the temperature was ramped from room temperature to 500 °C over 60 minutes, and held for 5 hours. After slowly cooling to room temperature, the samples were exposed to an additional pyrolysis at either 700 (700CST), 900 (900CST), or 1100 °C (1100CST) (ramping at approximately 10 °C/min.). Once again, the temperature was then held constant for 2 hours. After cooling, the samples were placed directly into coin cell batteries for testing. Since the 1100CSTs performed the best out of the pristine samples, some of these samples were soaked in a 6M KOH solution for 10 hours at 70 °C (KOH1100CST) which were tested in batteries as well.

CR2032-type coin cells were fabricated with the as-synthesized PM CSTs as the working electrodes, microporous polypropylene as the separator (Celgard 2300), and lithium metal foil as the counter electrode. The electrolyte used was 1M $LiPF_6$ in a 1:1 v/v EC/DMC solvent system, with 2 wt.% VC as an additive. All batteries were prepared in an Ar-filled VAC Omni-lab glovebox, and were tested vs. lithium from 0.01 to 3 V on an Arbin BT2000. CV data was collected using a Bio-logic VMP3 with a scan rate of 0.1 mV/s. The masses of the free-standing electrodes used for cycling performance characterization of 700CSTs, 900CSTs, 1100CSTs and KOH1100CSTs were 1.7 mg, 1.2 mg, 1.0 mg, and 0.5 mg, respectively. Scanning electron microscopy, and energy-dispersive X-ray spectroscopy characterization was performed using an FEI Nova Nano450SEM.

References

1. Endo, M., Kim, C., Nishimura, K., Fujino, T. & Miyashita, K. Recent development of carbon materials for Li ion batteries. *Carbon* **38,** 183–197 (2000).
2. Buiel, E. & Dahn, J. R. Li-insertion in hard carbon anode materials for Li-ion batteries. *Electrochim. Acta* **45** 121–130 (1999).
3. Romanos, J. *et al.* Nanospace engineering of KOH activated carbon. *Nanotechnology* **23,** 015401 (2012).
4. Lv, Y. *et al.* A comprehensive study on KOH activation of ordered mesoporous carbons and their supercapacitor application. *J. Mater. Chem.* **22,** 93–99 (2012).
5. Hwang, Y. J., Jeong, S. K., Nahm, K. S., Shin, J. S. & Stephan, A. M. Pyrolytic carbon derived from coffee shells as anode materials for lithium batteries. *J. Phys. Chem. Solids* **68,** 182–188 (2007).
6. Han, S., Jung, D., Jeong, J. & Oh, E. Effect of pyrolysis temperature on carbon obtained from green tea biomass for superior lithium ion battery anodes. *Chem. Eng. J.* **254,** 597–604 (2014).
7. Zheng, H., Qu, Q., Zhang, L., Liu, G. & Battaglia, V. S. Hard carbon: a promising lithium-ion battery anode for high temperature applications with ionic electrolyte. *R. Soc. Chem. Adv.* **2,** 4904–4912 (2012).

8. Zhang, F., Wang, K., Li, G. & Chen, J. Hierarchical porous carbon derived from rice straw for lithium ion batteries with high-rate performance. *Electrochem. Commun.* **11,** 130–133 (2009).
9. Yi, J. *et al.* Preparation of hierarchical porous carbon and its rate performance as anode of lithium ion battery. *J. Power Sources* **196,** 6670–6675 (2011).
10. Wang, J. & Kaskel, S. KOH activation of carbon-based materials for energy storage. *J. Mater. Chem.* **22,** 23710 (2012).
11. Guo, B. *et al.* Soft-Templated Mesoporous Carbon-Carbon Nanotube Composites for High Performance Lithium-ion Batteries. *Adv. Mater.* **23,** 4661–4666 (2011).
12. Dobele, G. *et al.* Formation of nanoporous carbon materials in conditions of thermocatalytic synthesis. *J. Anal. Appl. Pyrolysis* **103,** 173–180 (2013).

Author Contributions

B.C., C.S.O. and M.O. designed the experiments and wrote the manuscript. B.C. and R.I. worked on materials synthesis and characterization of morphology and composition. B.C. performed battery fabrication, galvanostatic charge-discharge measurements, voltage profiling, and CV measurements. Z.F. contributed to data analysis and analytical characterization. C.S.O. and M.O. managed the research team. All authors reviewed the manuscript.

Additional Information

Competing financial interests: The authors declare no competing financial interests.

How to cite this article: Campbell, B. *et al.* Bio-Derived, Binderless, Hierarchically Porous Carbon Anodes for Li-ion Batteries. *Sci. Rep.* **5**, 14575; doi: 10.1038/srep14575 (2015).